UNIVERSITY OF TWENTE.

PHYSICS OF FLUIDS

Master thesis

Splashing of Leidenfrost droplets

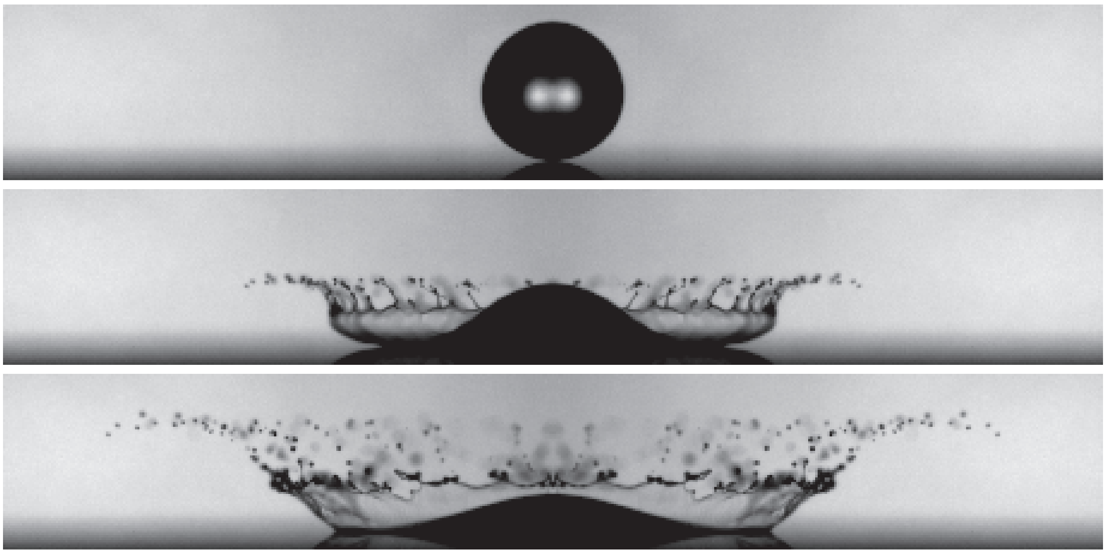

Author:
B. Geerdink

Supervisor:
Ir. H.J.J. Staat

Graduation committee:
Prof. dr. D. Lohse
Dr. C. Sun
Dr. A.T. Tran
Dr. ir. H. Wormeester

August 16, 2013

Abstract

When a droplet impinges on a smooth heated surface, which is heated above the liquid's boiling point, it either comes into contact with the surface (the *contact* regime), or it is separated from the surface by a vapor layer (the *film* or Leidenfrost regime). High-speed interferometric imaging is used to make a sharp distinction between both regimes. Increasing the droplet's impact velocity causes the droplet to splash and for each regime this transition to splash is determined experimentally. The transition in the *contact* regime is found to be at a lower critical Weber number as compared to that of the *film* regime. Both transitions depend on the temperature of the surface and are accounted for theoretically by extending the model from Xu *et al.* 2005 with the liquid-vapor phase transition. Additionally it is shown that the maximum deformation of a liquid drop, impacting a surface at high temperature, is consistent with the scaling law for the spreading factor $\Gamma \sim \mathrm{We}^{3/10}$ (Tran *et al.* 2013), which can be explained by taking into account the drag force of the vapor flow under the drop.

Contents

Chapter 1

Introduction

Drop impacts on solid surfaces can be seen in nature and everyday life. Most common are falling raindrops which impinge on a wide variety of surfaces like on roads, on the windshield of a car, in a puddle of rain or on leafs of different plants. These impacts can be generalized by referring them to as impact on a rough or smooth surface, on a liquid layer or on structured surfaces. Drop impacts are also a key element of various phenomena encountered in technological and industrial applications, such as in ink-jet printing and spray painting. The research described in this thesis is focused on the impact of droplets on a smooth solid surface.

Rioboo *et al.* [1] revealed six possible outcomes that can be observed when a droplet impinges on a solid dry surface at room temperature: deposition, prompt splash, corona splash, receding break-up, partial rebound and complete rebound. Usually when the impact velocity is very low, the droplet will just be deposited on the surface.

At sufficiently high impact velocities, *corona splashing* – which is also seen very often in research involving droplets splashing on a thin liquid film or on a liquid pool – can occur. This the rapid generation of a liquid lamella, which resembles the shape of a crown. At a certain moment the lamella breaks up and disintegrates in smaller droplets, as shown in (a).

When the smaller droplets are ejected directly from the region between the surface and the liquid in the spreading phase of the lamella – and the lamella is not directed upward as in the case of corona splashing – it is called *prompt splashing*, which is shown in (b).

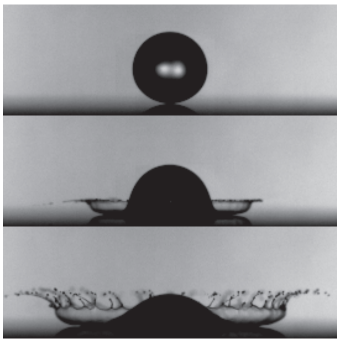

(a) Corona splash

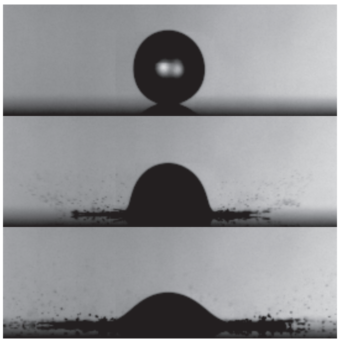

(b) Prompt splash

Receding break-up is the breaking up of the liquid into smaller droplets, when the liquid has reached its maximum extension and starts receding, while *(partial) rebound* is described by a droplet which impacts, spreads and (partially) bounces from the surface.

The mechanism of a droplet splashing on a dry solid surface has been studied for over a century now. In 1876, Worthington [2] was one of the first to investigate the phenomenon and since then, several theories have been proposed [3, 4], different splashing parameters have been introduced [5–9] at ambient air pressure, and more recently also the effect of the surrounding pressure has been investigated [10]. Nonetheless, the involving phenomena of splash and its mechanism are not yet fully understood.

Increasing the temperature of the surface on which a droplet impinges, gives rise to several other industrial applications. In processes such as rapid spray cooling of hot surfaces, fuel evaporation in internal combustion engines and cooling of electronic components, the process relies on droplet impact on a heated surface. The knowledge of splashing of droplets on heated surfaces, however, is lacking in the literature.

The objective of the research described in this thesis is to gain more insight into the temperature dependence of the transition from deposition to splashing. In order to investigate this, ethanol droplets impacting on a smooth surface with varying surface temperature are studied.

This thesis will start with more detailed background information about splashing and spreading in chapter 2. In chapter 3 the experimental setup which is used to perform the experiments is presented along with the techniques to be able to distinguish whether a droplet makes contact with the surface or not. The transition from deposition to splashing for variable impact velocities and surface temperatures is given in a detailed (T,We)-phase diagram in chapter 4, together with the results concerning the maximum spreading. This thesis concludes with chapter 5, where the results are summarized and discussed.

I would like to thank Tuan and Erik-Jan for the daily supervision and together with Chao for the encouraging discussions we had. Furthermore, I would like to thank Herbert Wormeester and Yoshiyuki Tagawa for taking place in my graduation committee and Detlef Lohse for giving me the opportunity to do this project in the Physics of Fluids group with all its resources.

Chapter 2

Background

In this chapter first some known splashing parameters at room temperature are described in section 2.1, followed by the influence of increasing the temperature of the surface (section 2.2). This chapter is concluded with a relatively new model, predicting the maximum spreading of droplets impacting on a heated surface (section 2.3).

2.1 Splashing parameters

Whether or not an impacting droplet makes a splash on a dry, solid surface at atmospheric pressure and at room temperature, is governed by a lot of parameters. Next to the typical impact-dependent parameters such as the diameter D_0 and velocity U_0 of the droplet, also the properties of the liquid like the density ρ, surface tension σ and (kinematic) viscosity ν play a role. Usually these parameters are combined into two dimensionless numbers: the Reynolds (Re) and Weber number (We), which are given by

$$\mathrm{Re} = \frac{U_0 D_0}{\nu} \qquad (2.1) \qquad\qquad \mathrm{We} = \frac{\rho U_0^2 D_0}{\sigma} \qquad (2.2)$$

The Reynolds number is a measure of the ratio between inertial and viscous forces, while the Weber number is the ratio between a fluid's inertia and its surface tension. Together they form a third dimensionless number, the Ohnesorge number (Oh):

$$\mathrm{Oh} = \frac{\sqrt{\mathrm{We}}}{\mathrm{Re}}. \qquad (2.3)$$

2.1.1 Roughness

Next to these dimensionless numbers, the roughness of the surface is another important parameter. Stow and Hadfield [5] were the first to empirically characterize the transition from spreading to splashing by presenting the splashing threshold as a constant, which is different for surfaces with a varying roughness:

$$\xi_c = \mathrm{Re}\cdot\mathrm{We}^2, \tag{2.4}$$

By rewriting this equation Mundo *et al.* [7] expressed their results into the often used *Mundo number*, K as:

$$\mathrm{Oh}\cdot\mathrm{Re}^{5/4} = \xi_c^{1/4} = K, \tag{2.5}$$

but did not find relevant differences for surfaces with different roughness, concluding that K is independent of roughness. However, Cossali *et al.* [8] later commented on this conclusion that the results from Mundo *et al.* were not inconsistent with those from Stow and Hadfield, because of the asymptotic value of the roughness they used.

Range and Feuillebois [9] confirmed the values of the splashing threshold from Stow and Hadfield using the same liquid and surface. For different liquids and surfaces, however, they argued that the splashing limit can be described by an empirical equation of the form

$$We_c = a\log^b \frac{R_0}{R_a}, \tag{2.6}$$

where a and b are fitting parameters and R_0/R_a is the ratio between the drop radius and the roughness amplitude. This equation was proposed by Wu [6], who pointed out that for small Oh the influence of viscosity effects is small and can thus be neglected.

The importance of the quality of the images used in experiments was stressed by Rioboo *et al.* [1]. They obtained different values for K than Mundo and Cossali, because of the high spatial and temporal resolution of the images they used, which allowed them to identify very small droplets.

2.1.2 Air pressure

Another important parameter was emphasized by Xu *et al.* [10]. They showed that a corona splash on a dry smooth substrate can be suppressed by decreasing the pressure of the surrounding gas, revealing the influence of the pressure on the splashing behavior.

In order to describe the pressure dependence on the splashing behavior, they consider two contributions to the stress on the expanding liquid: Σ_G and Σ_L. The first is due to the pressure of the gas on the liquid, which destabilizes the advancing front and deflects it upward. The latter is due to the surface tension of the liquid, which tends to keep the liquid layer intact. When both contributions become comparable, the spreading liquid becomes unstable and will eventually splash.

Because the air is assumed to be compressed, the stress due to the pressure of the gas, Σ_G, can be estimated by [10]

$$\Sigma_G \sim (\rho_G)(C_G)(V_e), \tag{2.7}$$

consisting of three parts: the density of the gas ρ_G, given by the ideal gas law, the speed of sound of the gas C_G and the velocity of the expanding liquid layer V_e:

$$\rho_G = \frac{PM_G}{k_B T} \quad (2.8) \qquad C_G = \sqrt{\frac{\gamma k_B T}{M_G}} \quad (2.9) \qquad V_e = \sqrt{\frac{R_0 U_0}{2t}} \quad (2.10)$$

where P is the atmospheric pressure, M_G, T and γ are the molecular weight, temperature and the adiabatic index of the gas, k_B is Boltzmann's constant, R_0 and U_0 are the initial radius and the impact velocity of the falling droplet and t is the time elapsed from the moment of impact.

The other stress, Σ_L, is approximated by the pressure due to the surface tension near the front of the advancing liquid. This is done by dividing the surface tension σ by the thickness of the layer d, which is characterized by the viscous length scale as $d = \sqrt{\nu t}$,

$$\Sigma_L = \frac{\sigma}{d} = \frac{\sigma}{\sqrt{\nu t}} \tag{2.11}$$

with ν the kinematic viscosity of the liquid and t the same time elapsed as in V_e.

The ratio of both stresses defines a "splashing parameter" κ:

$$\kappa \equiv \frac{\Sigma_G}{\Sigma_L} = \frac{PM_G}{k_B T}\sqrt{\frac{\gamma k_B T}{M_G}}\frac{\sqrt{R_0 U_0 \nu}}{2\sigma^2} \tag{2.12}$$

Considering the importance of the pressure and the roughness, it can be stated that using only the traditional dimensionless numbers is not enough to describe a splashing threshold. The more extensive parameter presented in equation 2.12 will be applied in section 4.3.

2.2 Leidenfrost temperature

When a droplet of liquid is deposited on a solid surface which is heated around the boiling temperature of the liquid, it spreads, boils and quickly vanishes (a process often called *contact boiling*). However, when the temperature of the surface is much higher than the boiling temperature, the droplet can be in a state that it is no longer in contact with the surface, but levitates above it on a layer of vapor (which is called *film boiling*). The lowest temperature at which this vapor layer is stable, is called the Leidenfrost temperature.

The effect of the insulating vapor layer on the evaporation rate of liquid droplets can be observed when the lifetime of a deposited droplet (τ) is measured as function of the temperature of the surface (T_s), as shown in figure 2.1.

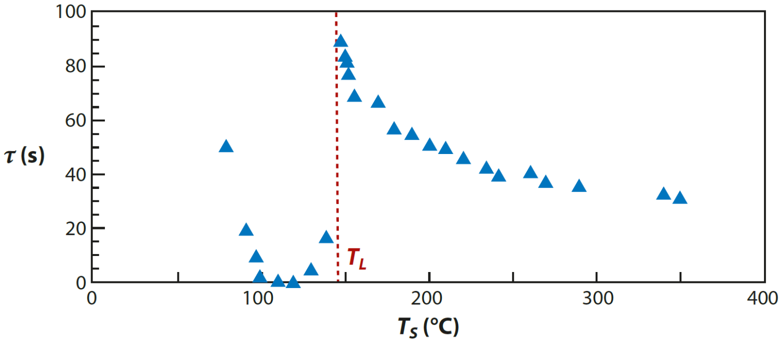

Figure 2.1: The lifetime τ of a 2 mm water droplet as a function of the temperature T_S of the surface, in this case a polished aluminum plate, on which it is deposited. Figure adapted from Biance *et al.* [11], taken from Quéré [12].

In figure 2.1 the sudden increase of the lifetime of the droplet is called the Leidenfrost temperature and is approximately 150 °C. Because the droplet is gently deposited onto the surface (*i.e.* it has no impact velocity) this is also known as the Leidenfrost temperature.

When the droplet falls onto the heated surface with a certain impact velocity, it is referred to as the *dynamic* Leidenfrost temperature. Tran *et al.* [13] show that this temperature increases with increasing We, as shown in figure 2.2: the dynamic Leidenfrost temperature is denoted by the violet dashed line, which separates the film and contact boiling regime (blue circles and red diamonds, respectively).

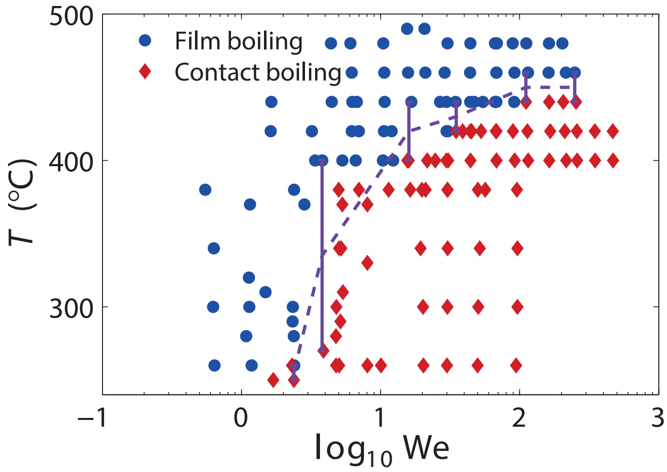

Figure 2.2: Phase diagram for water droplet impact on a heated smooth surface showing that the contact boiling regime (red diamonds) is separated from the film boiling regime (blue circles) by a transition that marks the dynamic Leidenfrost temperature (violet dashed line). Figure adapted from Tran *et al.* [13].

2.3 Maximum spreading

Also the maximum spreading of a droplet on a heated surface is often seen as an important factor for industry and technology. When a droplet does not splash, but spreads or bounces on a surface the spreading diameter will reach a maximum value D_m, as shown in figure 2.3.

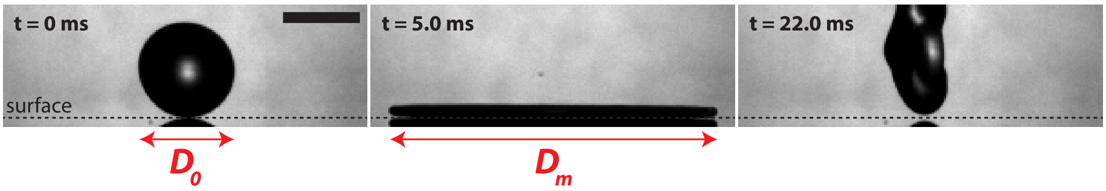

Figure 2.3: At typical rebound of a droplet which impacts on a heated surface. Having an initial diameter D_0 it spreads until it reaches a maximum deformation D_m (and eventually bounces from the surface).

The maximum spreading diameter is usually normalized by the initial drop diameter D_0 to obtain a dimensionless spreading factor $\Gamma = D_m/D_0$. Several theories have been postulated to predict this spreading factor at room temperature, of which one is presented in section 2.3.1. In section 2.3.2 a theory is presented in the case where the surface is heated and the impact is in the film boiling regime.

2.3.1 Gravity puddle model

The shape of a droplet being at rest on a plate (*i.e.* a puddle) is a result of the balance between gravity and surface forces. Therefore the thickness of the puddle should scale as the capillary length, which is given by

$$H = \sqrt{\frac{\sigma}{\rho g}}, \tag{2.13}$$

where g is the gravitational acceleration. The velocity of the droplet U_0, however, will be reduced to zero in a typical crashing time t^*, which is of the order D_0/U_0. This will result in a typical acceleration of the droplet of $a \sim U_0^2/D_0$. Clanet *et al.* [14] suggest that this effective acceleration experienced by the drop during its impact should be taken into account in equation 2.13, which results in

$$H = \sqrt{\frac{\sigma}{\rho a}} \sim \sqrt{\frac{\sigma D_0}{\rho U_0^2}}. \tag{2.14}$$

Together with volume conservation, which provides $D_0^3 \sim H D_m^2$, the following scaling law is obtained:

$$\Gamma \sim \mathrm{We}^{1/4} \tag{2.15}$$

This scaling law is in good agreement with the experimental data of Clanet *et al.* [14] dealing with impacting droplets of low viscosity on super-hydrophobic and partially wettable surfaces. It also holds for unheated surfaces of various wettability and roughness, as shown by Tsai *et al.* [15].

2.3.2 Vapor-induced spreading

On the other hand, when the surface is heated and the impact is in the film boiling regime, another scaling law is suggested by Tran *et al.* [16]. Again the liquid is modeled as a disk which now spreads on a layer of vapor of thickness scaled as h and area scaled as D_m^2, as shown in figure 2.4.

The heat that is required to evaporate the liquid is assumed to be conducted through this vapor layer, which allows to approximate the rate of heat transfer to the liquid using Fourier's law ($\dot{Q} = k_v \Delta T D_m^2/h$). By balancing the rate of vapor generation ($\dot{Q}/L$) with the rate of vapor which escapes the gap between the liquid and the solid, this results in:

$$\frac{k_v \Delta T D_m^2}{L h} \sim \rho_v V h D_m \tag{2.16}$$

where k_v and ρ_v are the thermal conductivity and density of the vapor, ΔT is the temperature difference between the liquid and the solid, L is the latent heat of evaporation and V is the radial velocity of the vapor flow.

The vapor flow is driven by an increase of the pressure under the drop, for which the dynamic pressure $\Delta P \sim \rho U_0^2$ is taken. Considering that the thickness of the vapor layer is very small, this flow is viscous and can be described by the lubrication approximation:

$\partial_x P \sim \mu_v \partial_z^2 V$ (with ∂_x and ∂_z the derivatives in radial and vertical direction). By taking into account the typical length scales in the horizontal and vertical direction (D_m and h) this results in:

$$\frac{\rho U_0^2}{D_m} \sim \frac{\mu_v V}{h^2} \tag{2.17}$$

where μ_v is the dynamic viscosity of the vapor.

Finally the viscous vapor flow exerts a drag force on the liquid, which is approximated by $\tau_v D_m^2 \sim \mu_v (U/h) D_m^2$ (with τ_v the viscous shear stress of the vapor flow). This drag force is balanced by capillarity, $(\sigma/H)D_m^2$, which together with volume conservation will result in:

$$\sigma \frac{D_m^2}{D_0^3} \sim \frac{\mu_v V}{h} \tag{2.18}$$

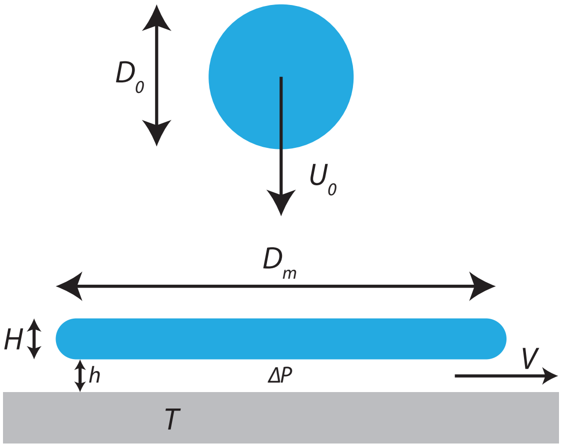

Figure 2.4: Schematic of a droplet with diameter D_0 which impacts on a heated surface (temperature T) with impact velocity U_0 and spreads until a maximum diameter D_m and thickness H. The drops spreads on a vapor layer of thickness h and vapor flows outward with velocity V due to the pressure increase ΔP.

When the dimensionless variables $\Gamma = D_m/D_0$, $\tilde{V} = V/U_0$ and $\tilde{h} = h/D_0$ are used, equation 2.16-2.18 can be combined and rewritten as:

$$\Gamma^2 \sim \tilde{h}^4 \mathrm{St}\mathrm{Pe} \tag{2.19}$$

$$\Gamma\tilde{V} \sim \tilde{h}\mathrm{St} \tag{2.20}$$

$$\tilde{V} \sim \Gamma^2 \tilde{h}\frac{\mathrm{St}}{\mathrm{We}} \tag{2.21}$$

where St and Pe are the dimensionless Stokes and Peclet number, given by
$\mathrm{St} = \rho D_0 U_0/\mu_v$ and $\mathrm{Pe} = \rho_v L D_0 U_0/k_v \Delta T$.

This system of equations is solved to obtain the final result for the spreading factor:

$$\Gamma \equiv \frac{D_m}{D_0} \sim \left(\frac{\mu_v k_v \Delta T}{\rho_v \sigma L D_0}\right)^{1/10} \mathrm{We}^{3/10} = \beta \mathrm{We}^{3/10} \tag{2.22}$$

Tran *et al.* [16] mention that their experimental results are consistent with this 3/10-scaling law for large We. For smaller We these results deviate from it and are closer to the previously mentioned 1/4-scaling law (equation 2.15), despite the fact it is derived considering unheated surfaces. Both scaling laws are also checked for consistency for the data obtained in the experiments described in this thesis in section 4.4.

Chapter 3

Measurement techniques

In order to study the splashing behavior of droplets impinging a (heated) surface an experimental setup is used consisting of three main components: a way to generate droplets of reproducible size, a plate which can be heated and an imaging system to record the impact. This setup (figure 3.6) and examples of typical recordings are given in section 3.1. Another setup which is used to distinguish whether a droplet touches the surface or not by means of interference, is presented in section 3.2.

3.1 Main setup

By pushing liquid out of a syringe (Hamilton Gastight 5.0 mL) with a syringe pump (Harvard PHD 2000) at an infuse rate of 50 µl/min through a flat-tipped needle, a droplet is gently formed at the tip of this needle. When the weight of the droplet exceeds the surface tension, that keeps the droplet connected to the needle tip, the droplet will detach from the needle. To prevent the liquid from crawling up before the detachment, resulting in a major decrease in the reproducibility, the needle is coated with an oleophobic coating (3M Novec 1700).

Once the droplet detaches from the needle, it has a diameter D_0 and falls onto a surface with a certain impact velocity U_0. With the use of a high speed side view camera (Photron Fastcam SA1.1) the impact is recorded and the splashing behavior of the impacting droplet is studied. In addition to the qualification of this behavior, the diameter and impact velocity of the droplet are obtained from these recordings. A number of subsequent images before the impact are taken and an ellipse is fitted to the drop, as shown in figure 3.1: (a) shows the original image and in (b) the fitted ellipse is drawn. To obtain the diameter of the droplet, the mean value of both radii of the ellipse of each image is taken, followed by taking the average of these mean values of all subsequent images. By subjecting the center of each ellipse of the images to a linear fit the impact velocity is computed.

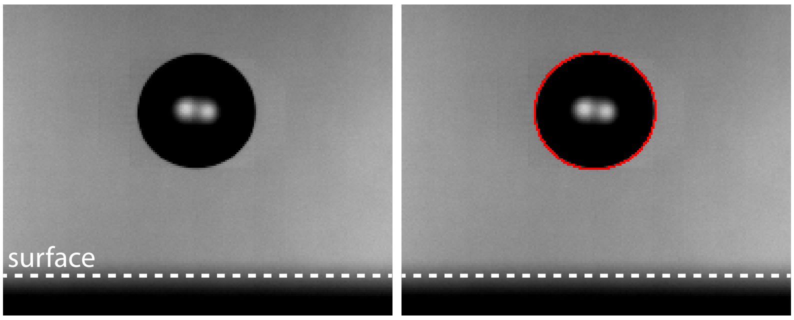

(a) (b)

Figure 3.1: A typical droplet (a) and its fitted ellipse drawn in red (b). The white dashed line represents the surface.

Figure 3.2 shows typical side view images of impacts of an ethanol droplet impacting on sapphire at room temperature. When the velocity of the drop is increased the type of impact changes from deposition of the droplet (figure 3.2(a)) to splashing (figure 3.2(b)) and at even higher impact velocity to clear corona splashing, as shown in figure 3.2(c).

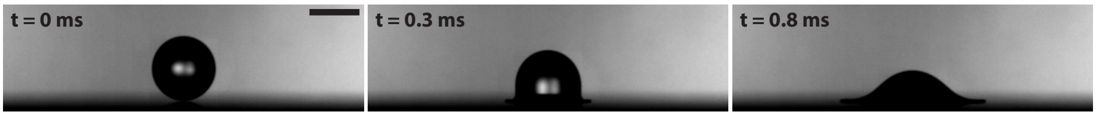

(a) We = 339

(b) We = 471

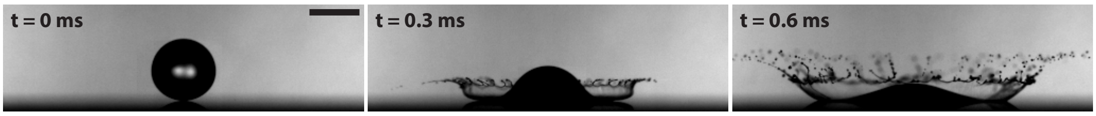

(c) We = 1401

Figure 3.2: Three typical time series of a droplet impacting at room temperature. At some impact velocity the droplet is splashing (b), instead of being deposited on the surface (a). At even higher impact velocities (c) a clear corona splash is visible. The scale bar indicates 2 mm.

The impact velocity of the drop is changed by altering the height of the needle by sliding it along a rail. Whenever the needle is too high, there is too much influence of ambient disturbances and the droplet will not fall on the desired position on the surface on which the camera is in focus.

To minimize the influence of the disturbances on the droplet during its fall a 112 cm long metal tube is used to shield the trajectory of the droplet. An adjustable diaphragm at the end of the tube will only let drops through which are falling through the center.

To look at the splashing behavior in greater detail a bottom view is required. This is possible by using a transparent plate which can be heated. As a surface a 3 mm thick polished sapphire disk (Goodfellow Cambridge Limited) having a diameter of 10 cm is used. This disk is placed onto a custom made brass plate, held by a custom made stainless steel holder (figure 3.5). Both the brass plate as its holder are provided with a 4 cm hole in the center, which makes it possible to make bottom view recordings. The bottom view camera (Photron Fastcam SA-X) is synchronized with the side view camera. The light necessary to make the bottom view recordings is diffused by a ceramic plate which has a hole in the middle in order for the droplets to fall through. This diffuser is positioned in between the surface and the needle. Side view recordings accompanied by their synchronized bottom view recordings of typical droplet impacts are shown in figure 3.3.

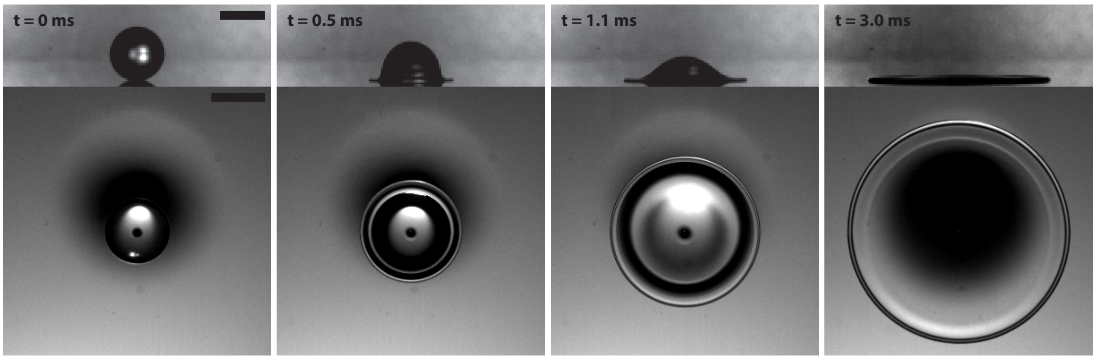

(a) We = 170

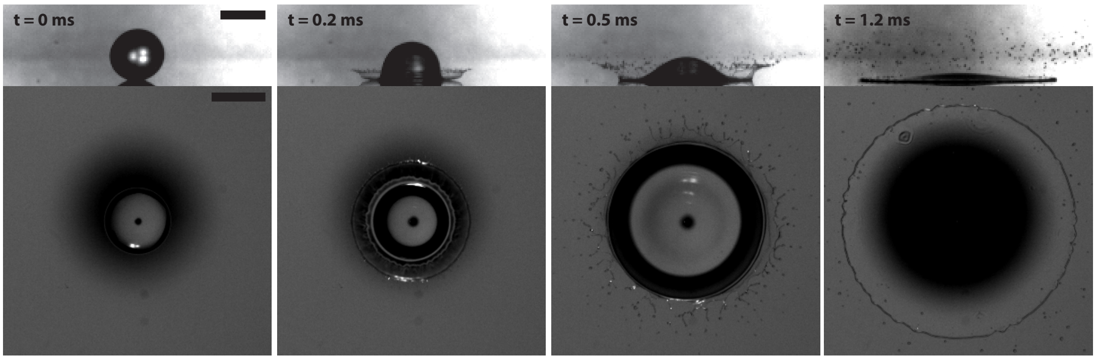

(b) We = 761

Figure 3.3: Two side view time series of typical drop impacts, accompanied by their synchronized bottom views. The scale bars indicate 2 mm.

Along with the Weber number, the second control parameter is the temperature, T. Six cartridge heaters and a thermocouple are inserted into the brass plate to heat the sapphire disk and to control the temperature with a digital temperature controller (Omega CN9000A). The actual temperature of the disk compared to the set point temperature of the temperature controller is measured with a temperature probe (Dostmann Electronic P710). To minimize unwanted heat exchange between the brass plate and the holder, both are separated by three glass beads.

Increasing the temperature of the surface leads to a different behavior of droplets impacting on this heated surface. Two typical impacts are shown in figure 3.4: one at relatively low impact velocity (a), where a droplet bounces from the surface and one at high impact velocity (b), where a droplet splashes.

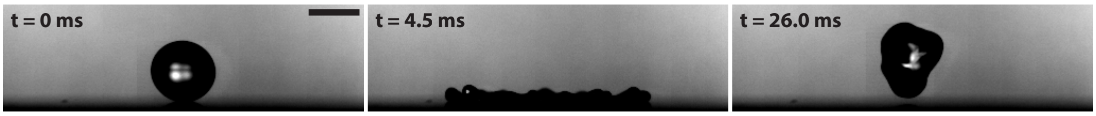

(a) We $= 85, T = 200$ °C

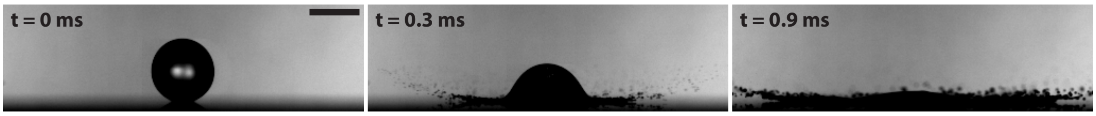

(b) We $= 1156, T = 200$ °C

Figure 3.4: Two typical time series of a droplet impinging at a heated surface, resulting in (a) bouncing and (b) splashing. The scale bars indicate 2 mm.

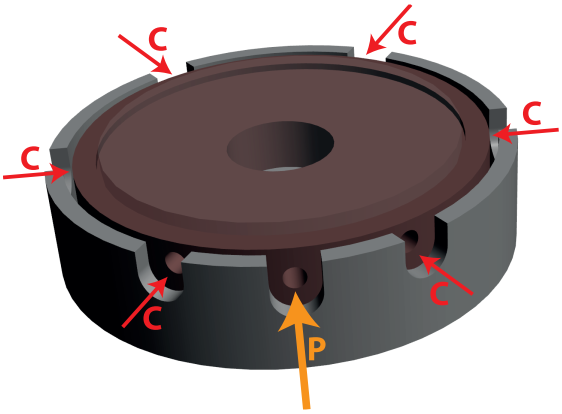

Figure 3.5: Custom made heater and holder. The arrows indicate the different holes in which the cartridge heaters (C) and the temperature probe (P) can be inserted.

Figure 3.6 shows a schematic overview of the complete setup which is used to measure the splashing behavior of droplets impacting on a sapphire surface and to quantify the two control parameters, the Weber number and the temperature.

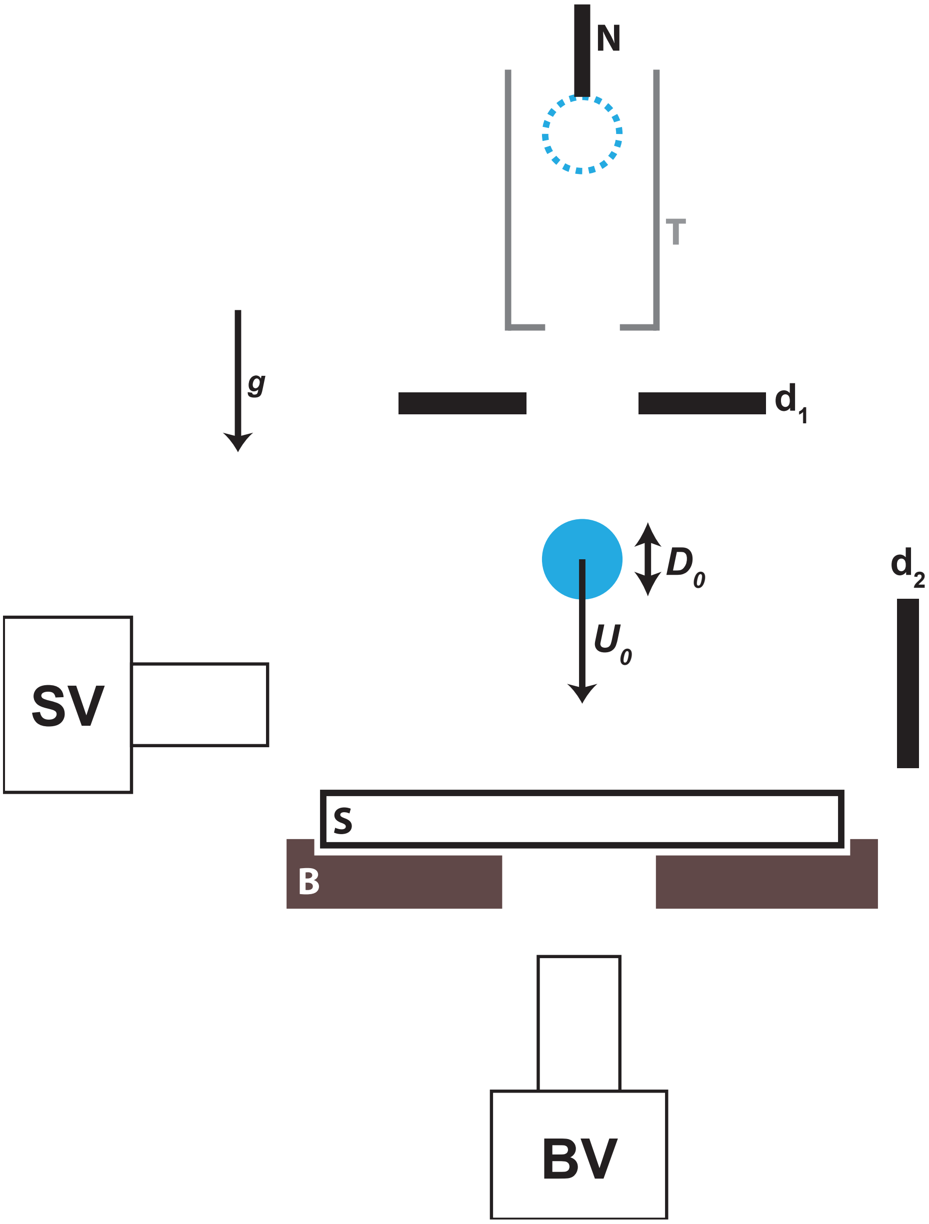

Figure 3.6: Schematic of the main setup which is used. A drop (with diameter D_0) detaches from a needle (N) and falls through a ceramic diffusive plate (d_1) onto a (heated) transparent surface (S), with velocity U_0. The brass plate (B, figure 3.5) is able to heat the surface. Side view (SV) light is supplied from behind (and diffused by) d_2 and bottom view (BV) light is supplied from above (and diffused by) d_1.

3.2 Interference

In this section the alternative setup is described, which is used to distinguish whether a droplet makes contact with the surface or not. When a droplet does not contact the surface, it is due to the fact that the temperature of the surface causes enough liquid to evaporate to form a stable liquid film just before impact. This way a vapor layer is formed on which the remaining liquid will impact, instead of on the solid surface. When the solid is transparent light can travel through it freely until it reaches an interface. A schematic of a liquid which is separated from a solid by a gas layer is given in figure 3.7.

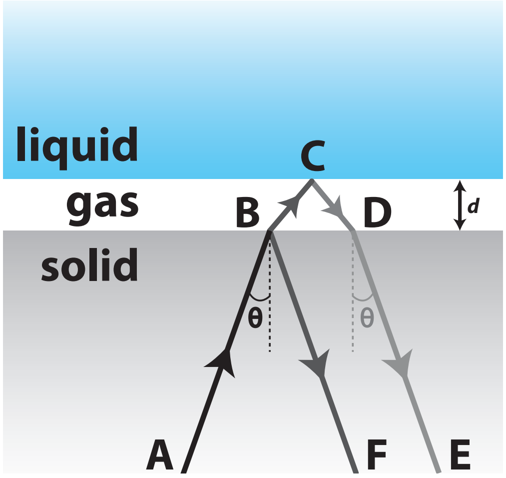

Figure 3.7: A liquid layer separated from the solid by a gas layer. Light travelling from A to B (at an angle θ) is reflected to F and refracted to point C. At C the light is reflected to point D, where it is refracted to E.

When light travels from the transparent solid to a liquid through a gas layer it is partially refracted (path AB → BC) and partially reflected (AB → BF) at the solid-gas interface. The refracted light then travels until it – again – is partially reflected (BC → CD) and refracted (BC → into liquid) at the gas-liquid interface. At this point the light is (partially) reflected to point E through point D.

The optical path difference between the path ABF and the path ABCDE will result in constructive and destructive interference, where the criterion for the constructive interference is:

$$2n_g d \cos\theta = m\lambda \tag{3.1}$$

where θ is the angle the incident light makes with the normal of the solid surface at B, d is the thickness of the gas layer and n_g (≈ 1) is the refractive index of the gas.

Whenever a gas layer is not present between the solid and the liquid, no interference pattern will be visible and most of the light is transmitted through the liquid, while almost no light is reflected back. This way a clear distinction can be made whether a droplet touches the surface or not.

In order to be able to visualize the interferometry, another setup is used, as shown in figure 3.8. Blue laser light ($\lambda = 488\pm5$nm) with a beam diameter of 0.7 mm coming from a continuous wave laser (iFLEX-Gemini) is expanded with a beam expander (Edmund Optics). With a beam splitter the light is directed towards the surface. Once the light is reflected back, it will travel through the beam splitter towards a mirror where it is recorded by the high speed bottom view camera (Photron Fastcam SA-X). Droplets will fall on a 3.15 mm thick sapphire disk (Edmund Optics) having a diameter of 50.8 mm, which is held by a custom made aluminum holder in which two cartridge heaters and a thermocouple are inserted. This way the surface is heated and the temperature is controlled with a digital temperature controller (Omega CN9000A). Again the actual temperature of the disk compared to the set point temperature of the temperature controller is measured with a temperature probe (Dostmann Electronic P710).

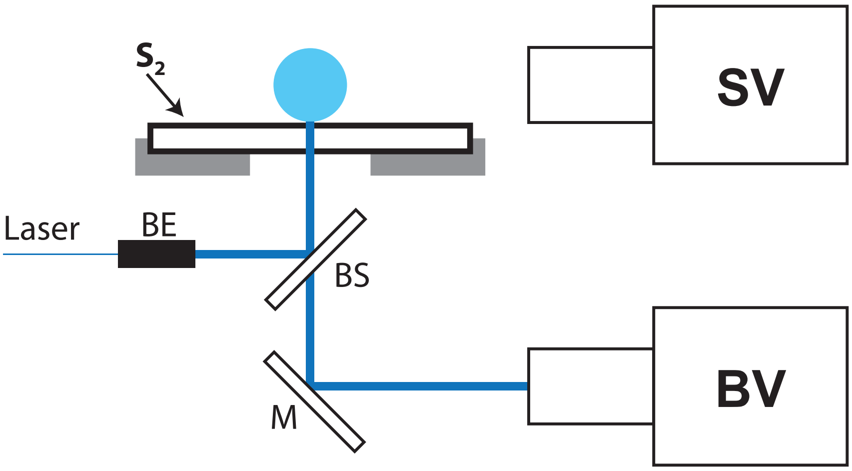

Figure 3.8: Interference setup: blue laser light ($\lambda = 420$ nm) is expanded with a beam expander (BE) and directed towards the sapphire surface (S_2) with a beamsplitter (BS) and is – depending on whether the droplet contacts the surface or not – reflected by the mirror (M) into the bottom view camera (BV), which is synchronized with the side view camera (SV).

The difference between touching and non-touching is shown in figure 3.9: in figures 3.9(a) and 3.9(b) the droplet touches the surface, while in figure 3.9(c) the droplet is not touching the surface as it is separated by a layer of vapor.

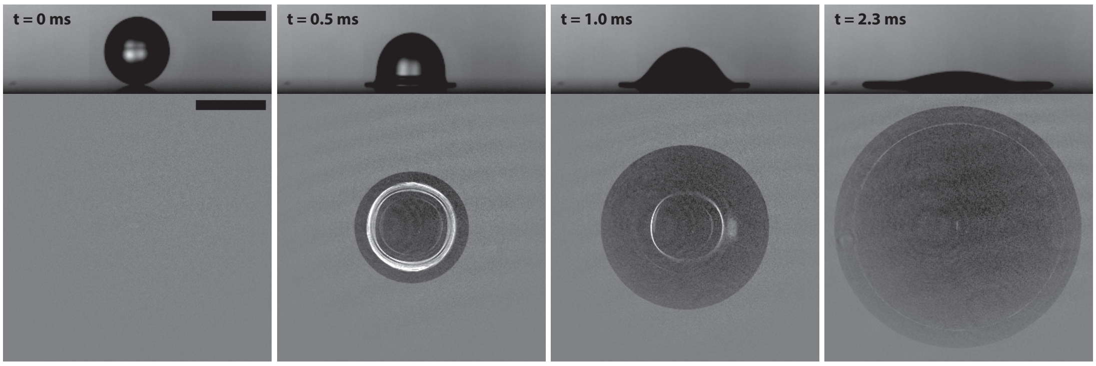

(a) $T = 20°\text{C}$, contact

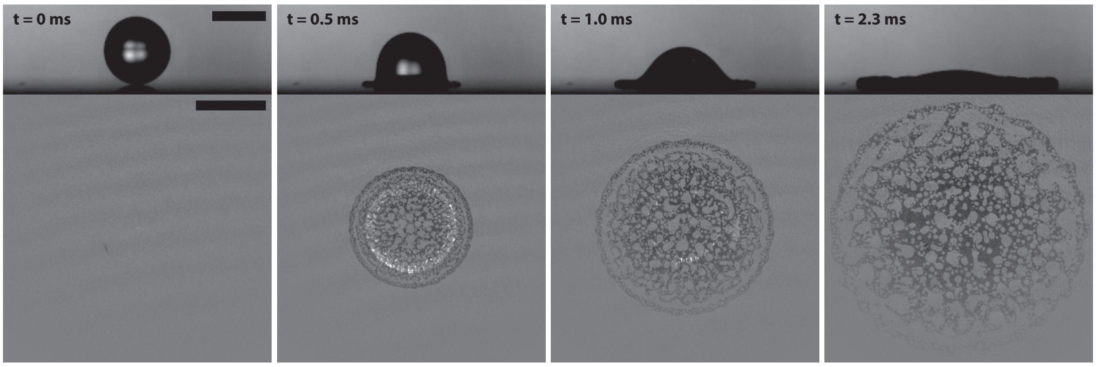

(b) $T = 150°\text{C}$, contact

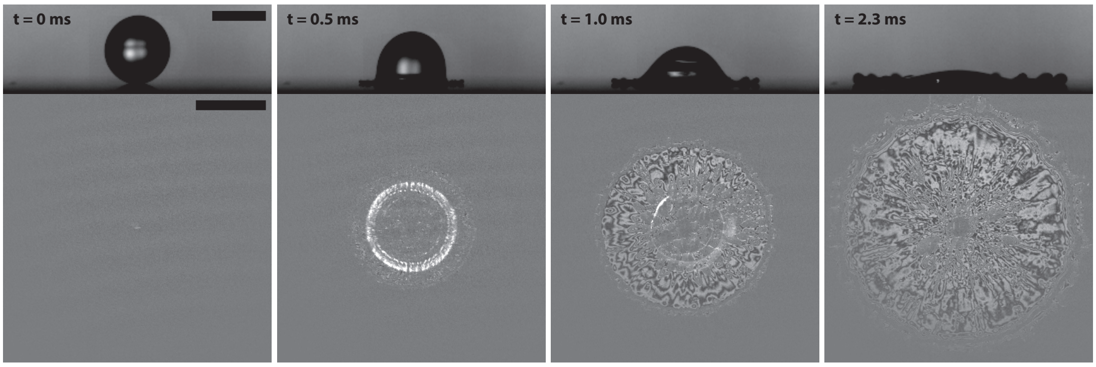

(c) $T = 200°\text{C}$, no contact

Figure 3.9: Typical side view recordings accompanied by their interferometric bottom view recordings of an ethanol droplet impacting on sapphire (We $\approx$ 135) at different temperatures. In (a) and (b) the droplet is in contact with the surface, while at (c) the interference pattern is visible (*i.e.* the droplet is separated from the solid by a vapor layer). All scale bars indicate 2 mm.

Chapter 4

Results

In this chapter first several impact phenomena encountered in this research are described (section 4.1), followed by the presentation of a detailed (T,We)-diagram (section 4.2) and further investigation of the transitions from deposition to splash in section 4.3. This part is concluded with section 4.4, which is about the maximum deformation of the droplet at high temperatures.

The results of the experiments presented in this chapter are performed with droplets of ethanol having an initial diameter of 2.53 ± 0.05 mm. Varying the release height of the droplet provides impact velocities ranging from 0.81 to 4.90 m/s. Using $\rho = 789$ kg/m^3 and $\sigma = 22$ mN/m, the corresponding range of Weber numbers is $58 \leq \mathrm{We} \leq 2273$. The temperature of the smooth sapphire surface is varied between room temperature (20 °C) and 432 °C.

A distinction is made whether a droplet splashes or not, where splashing is defined as the event occurring when a droplet hits a surface and an acceleration of ejected smaller droplets is observed. At the moment of impact the droplet can have direct contact with the surface or it is separated from the surface by a vapor layer, which is distuinguished by the interferometric measurement technique described in section 3.2. Using this technique, the dynamic Leidenfrost temperature, T_L, is measured to be between 150 and 175 °C, resulting in an estimated T_L of 162.5 °C for all We.

4.1 Impact phenomena

When a drop of ethanol impinges on a smooth sapphire surface at room temperature and at a relatively low impact velocity, the droplet will just spread, remain on the surface and no splashing is observed, which is shown in figure 4.1(a). Increasing the temperature above the dynamic Leidenfrost temperature, results in a droplet which will spread on the vapor film first, after which it recedes and completely bounces off the surface, as can be seen in figure 4.1(b) and also in Richard and Quéré [17]. In this case, the surface tension is able to keep the liquid together. However, when the impact velocity is slightly increased, inertia becomes more dominant compared to the surface tension and the droplet will break up into smaller droplets when it recedes. This receding break-up is displayed in figure 4.1(c).

Looking at droplet impact at room temperature, while increasing the impact velocity, the droplet will eventually produce a corona splash, as shown in figure 4.1(d). The transition from deposition to splash, however, is different for each surface temperature. This is illustrated in figure 4.2: starting with a splashing droplet (a), increasing the temperature results in the droplet to be deposited on the surface (b). When the temperature is increased above T_L the droplet will produce a splash again.

In the low velocity regime, however, there is also a similar effect on the splashing behavior, displayed in figure 4.3: while the droplet is splashing at a temperature just above the Leidenfrost temperature (b), it is not splashing when the temperature is below (a) and well above T_L (c), where deposition and bouncing behavior is observed, respectively.

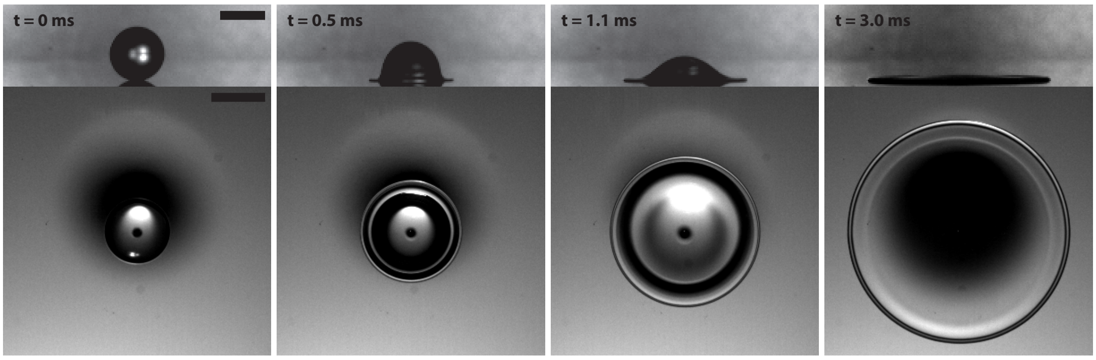

(a) We $= 170, T = 20$ °C, deposition

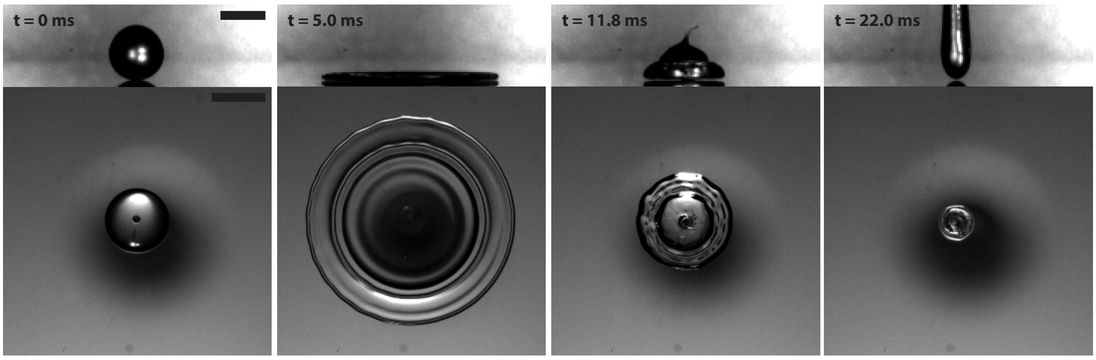

(b) We $= 83, T = 265$ °C, bouncing

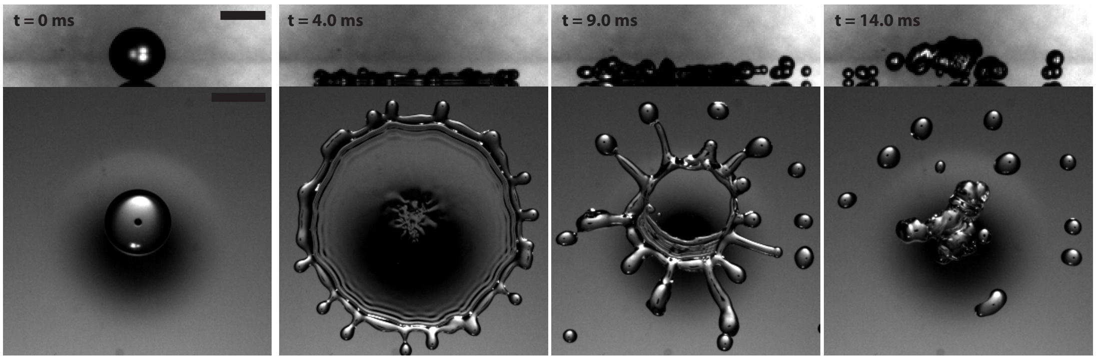

(c) We $= 128, T = 265$ °C, receding break-up

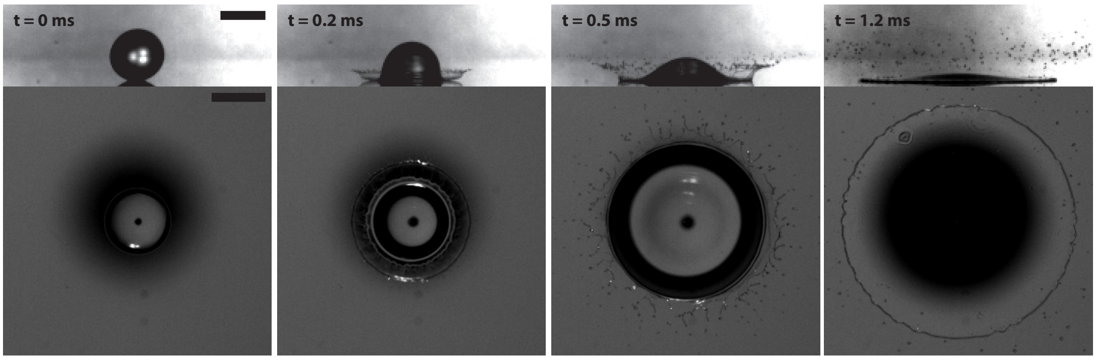

(d) We $= 761, T = 20$ °C, corona splashing

Figure 4.1: Four typical impact phenomena: (a) deposition, (b) bouncing, (c) receding break-up and (d) corona splashing. The scale bars indicate 2 mm.

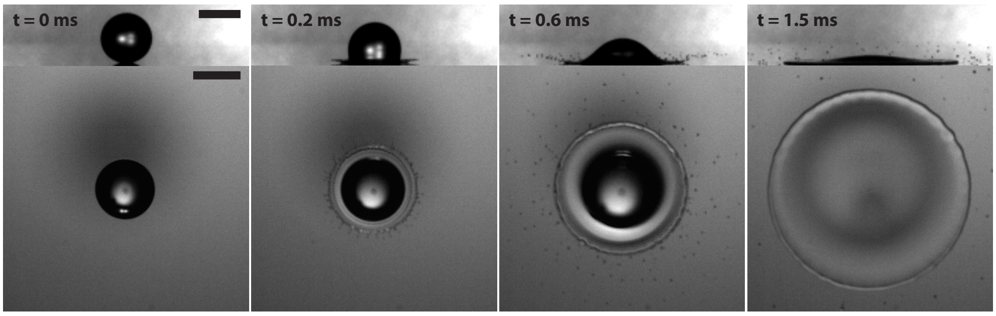

(a) $T = 20$ °C, splashing

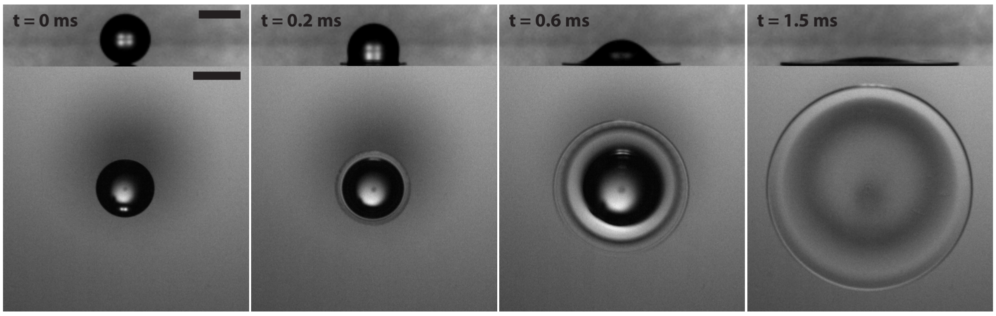

(b) $T = 94$ °C, deposition

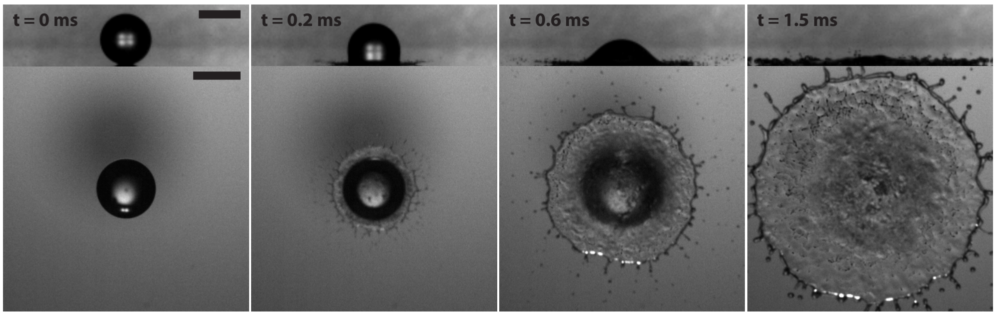

(c) $T = 185$ °C, splashing

Figure 4.2: The change from splashing to deposition and back to splashing, solely by changing the surface temperature. The corresponding We numbers are: (a) We = 456, (b) 458 and (c) 461. The scale bars indicate 2 mm.

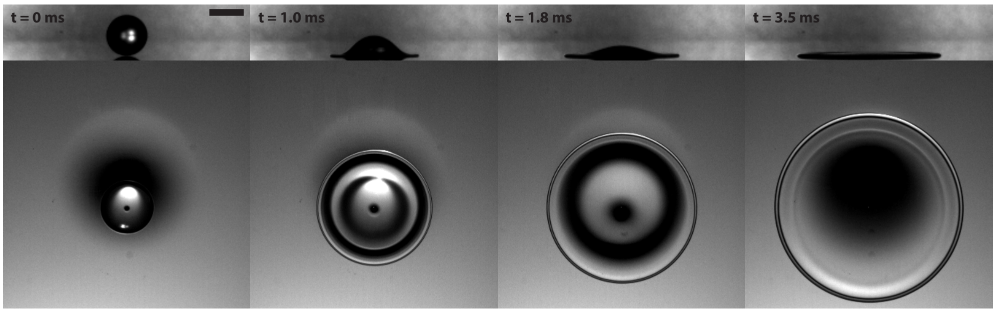

(a) $T = 20$ °C, deposition

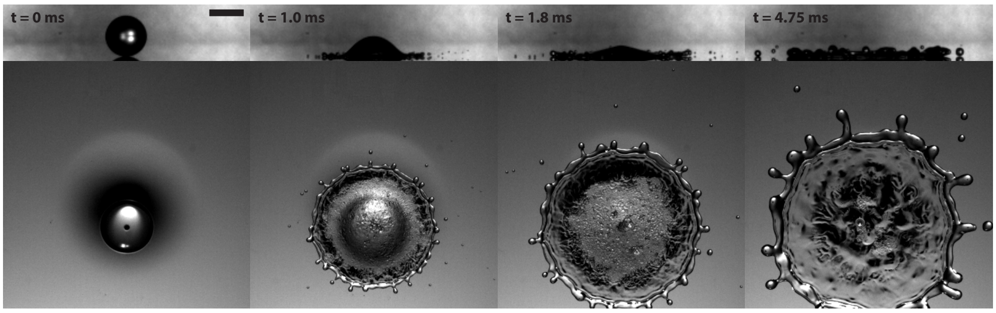

(b) $T = 185$ °C, splash

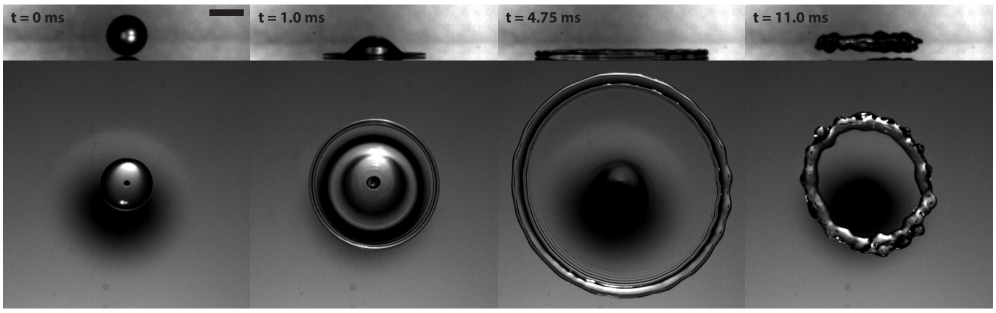

(c) $T = 352$ °C, bounce

Figure 4.3: The change from deposition to splashing to bouncing, by changing the surface temperature only. The corresponding Weber numbers are: (a) We = 170, (b) 170 and (c) 175. The scale bars indicate 2 mm.

The last impact phenomenon is observed when the temperature of the surface and the impact velocity are both reaching the limit of this research, $T = 432$ °C and We ≥ 1000. For these values a stable liquid film is produced which is able to survive a relatively long time before it ruptures, as shown in figure 4.4.

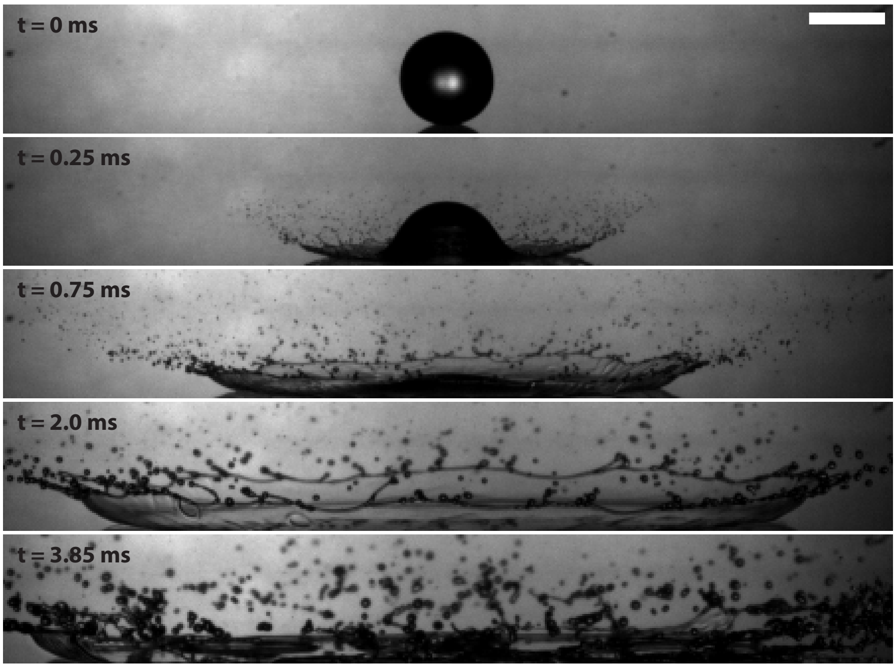

Figure 4.4: A droplet impacting at $T = 432$ °C and We = 1029, producing a stable liquid film. The scale bars indicate 2 mm.

4.2 Phase diagram

All the impacts recorded in the experiments are classified into four regimes. When the droplet is in contact with the surface and does not splash, it is called *deposition* and is shown in figure 4.1(a). However, when it does splash it is referred to as *contact splash*, which is shown in figure 4.1(d). If the droplet does not splash and is not in contact with the surface (*i.e.* separated by a vapor layer) it is called *bounce* (also including the receding break-up behavior). This regime is presented by figure 4.1(b) and 4.1(c). When it does splash without surface contact it is referred to as *film splash*, shown in figure figure 4.2(c), figure 4.3(b) and 4.4.

All the measurements are classified according to the aforementioned four regimes and presented in a (T,We)-diagram, as shown in figure 4.5.

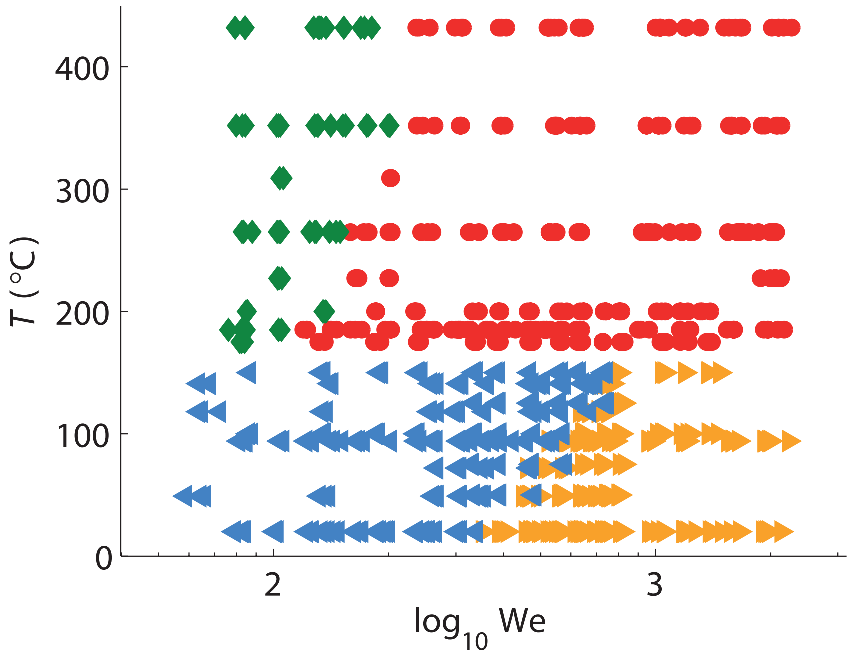

Figure 4.5: Phase diagram of impacting ethanol droplets on smooth sapphire, showing four regimes: deposition regime (blue triangles), contact splash regime (orange triangles), bounce regime (green diamonds) and film splash regime (red circles). The dynamic Leidenfrost temperature ($T_L = 162.5$ °C) separates the contact and no contact regimes.

As can be seen, the transition from deposition to contact splash (hereinafter referred to as the *deposition transition*), as well as the transition from bounce to film splash (*i.e.* the *bounce transition*), are both dependent on the surface temperature. This was already stressed in figure 4.2 and figure 4.3. These transitions are investigated in the next section.

4.3 Splash transitions

The deposition and bounce transitions are subject to the "splashing parameter" κ, given by equation 2.12. This parameter is not known *a priori*, but is used as a fitting parameter and should be of order unity. The equation can be rewritten as follows:

$$\kappa = \frac{P}{\sigma}\sqrt{\frac{M_G\gamma}{k_BT}}\sqrt{\frac{R_0U_0\nu_l}{2}} \tag{4.1}$$

In order for the equation to be applicable to the phase diagram of figure 4.5, the values of the variables in equation 4.1 have to be chosen carefully. For both the deposition transition as the bounce transition, ν_L will be that of ethanol at room temperature: $1.36 \cdot 10^{-6}$ m^2/s. Here it is assumed that the viscosity of the liquid remains constant during impact despite the presence of the heated surface. On the other hand the surface tension, σ, will be different for both transitions. For the deposition transition this will be the value at room temperature (22 mN/m), while for the bounce transition the value at the boiling temperature of ethanol (78.15 °C) is taken: 17.55 mN/m. The molecular weight M_G of air is used for the deposition transition, whereas for the bounce transition that of ethanol vapor is taken, being 29 and 46 g/mol respectively. For the deposition transition the value of the adiabatic index γ is taken to be 1.4. while for the bounce transition this is 1.13. The atmospheric pressure P is the same for both transitions.

In figure 4.6 the values for κ in the deposition (blue triangles) and contact splash regime (orange triangles) are given as function of $\sqrt{R_0U_0/T}$. By taking the maximum value for the lower regime and the minimum value for the upper regime, a transition value for κ is determined. This results in $\kappa = 0.79 \pm 0.02$.

For the transition between the bounce (green diamonds) and film splash regime (red circles) it is assumed that the maximum temperature at which the ethanol vapor can be, is at the boiling temperature ($T_{\text{boil}} = 351.3$ K).

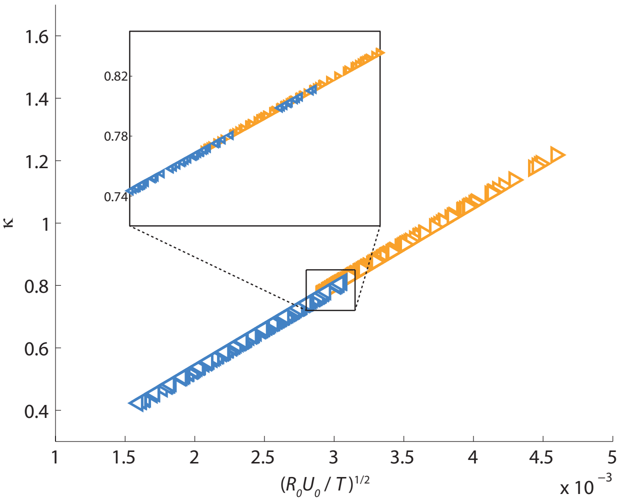

Figure 4.6: Values of κ (equation 4.1) given for the deposition (blue triangles) and contact splash regime (orange triangles). The resulting transition value for $\kappa = 0.79 \pm 0.02$.

In figure 4.7 the corresponding values for κ are given as function of $\sqrt{R_0 U_0}$. Determining the transition value in the same way as for the deposition transition, results in $\kappa = 0.82 \pm 0.06$.

By taking the transition values from figure 4.6 and 4.7, the corresponding Weber numbers can be calculated. For the bounce transition this results in a straight line, as there is no dependence on T. Both transitions are presented in the phase diagram to illustrate the extent to which the theory matches the experiments, as shown in figure 4.8.

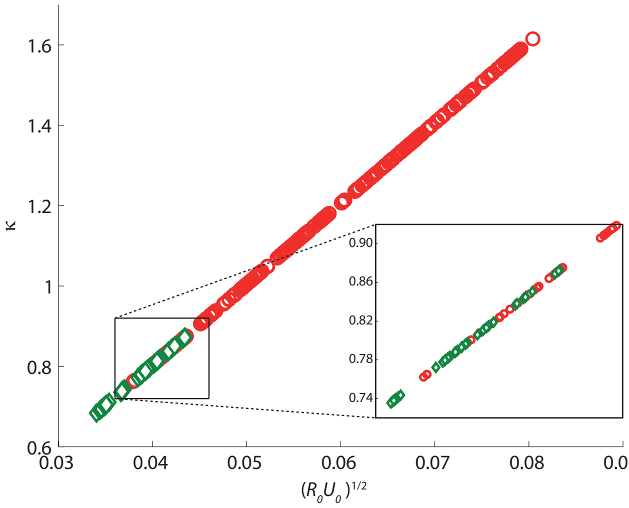

Figure 4.7: Values of κ (equation 4.1) given for the bounce (green diamonds) and film splash regime (red circles) at a constant temperature (T_{boil}). The resulting transition value for $\kappa = 0.82 \pm 0.06$.

As can be seen, the obtained transition line below the Leidenfrost temperature seems to follow the experimental data accurately, while the transition line above T_L does not. However, when it is assumed that the vapor can be at temperatures above T_{boil}, this transition line will depend on We, as shown in figure 4.10.

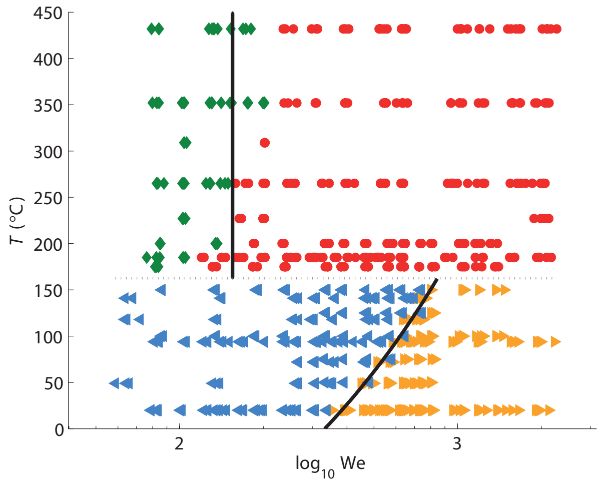

Figure 4.8: Two values for κ presented in the phase diagram. For the deposition transition $\kappa = 0.79$ (figure 4.6) is used. For the bounce transition, a constant temperature T_{boil} is used resulting in $\kappa = 0.74$ (figure 4.7).

In figure 4.9 the corresponding values for κ are given as function of $\sqrt{R_0 U_0 / T}$, which results in a value the bounce transition of $\kappa = 0.66 \pm 0.02$. Again, with this alternative transition value, the corresponding Weber numbers are calculated and inserted into the phase diagram, to illustrate the extent to which the theory matches the experiments.

The result is shown in figure 4.10. As can be seen, the transition line above T_L follows the experimental data more accurately than under the assumption that the vapor cannot be at a higher temperature than T_{boil}.

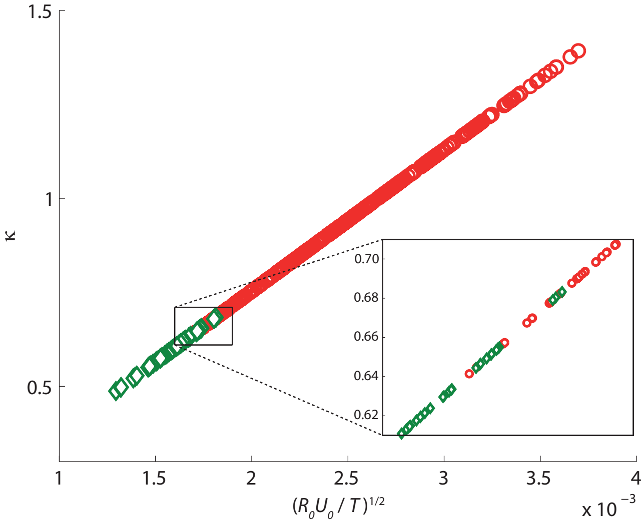

Figure 4.9: Values of κ (equation 4.1) given for the bounce (green diamonds) and film splash regime (red circles). The resulting transition value for $\kappa = 0.66 \pm 0.02$.

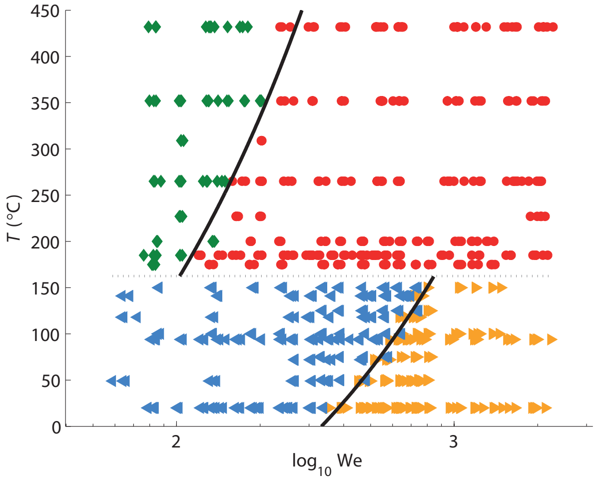

Figure 4.10: Two values for κ presented in the phase diagram. For the deposition transition $\kappa = 0.79$ and for the bounce regime $\kappa = 0.66$ is used.

4.4 Maximum deformation

To check whether the maximum deformation scales as $\mathrm{We}^{3/10}$ (equation 2.22), only a few droplets in a limited range of We and T are qualified to be analyzed, as bouncing or a formation of a stable liquid film is required. As the latter only occurs at $T = 432$ °C, only bouncing droplets at this temperature are considered. An example of the formation of a liquid film is given in figure 4.4, where the film is formed and spreads until a maximum extension is reached, followed by the rupture of the liquid film. The maximum extension (or deformation) of this liquid film, just before it starts to rupture, is determined as shown in figure 4.11.

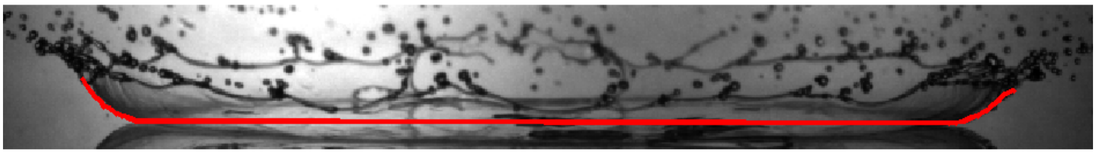

Figure 4.11: Illustration of the maximum extension of the liquid film, just before rupturing, represented by the red line.

The maximum deformation is divided by the initial diameter of the droplet before impact, D_0, and plotted on a log-log scale versus the Weber number. This way it can be compared with the vapor-induced 3/10-scaling law (section 2.3.2), along with the 1/4 scaling law, which is based on the gravity puddle model (section 2.3.1). The result is given in figure 4.12.

As can be seen for $\mathrm{We} > 300$, the data taken from Tuan *et al.* [16] combined with the measurements of ethanol droplets on sapphire are in line with $D_m/D_0 \sim \mathrm{We}^{3/10}$ scaling law, presented in section 2.3 by the solid line, which has a prefactor of 0.96.

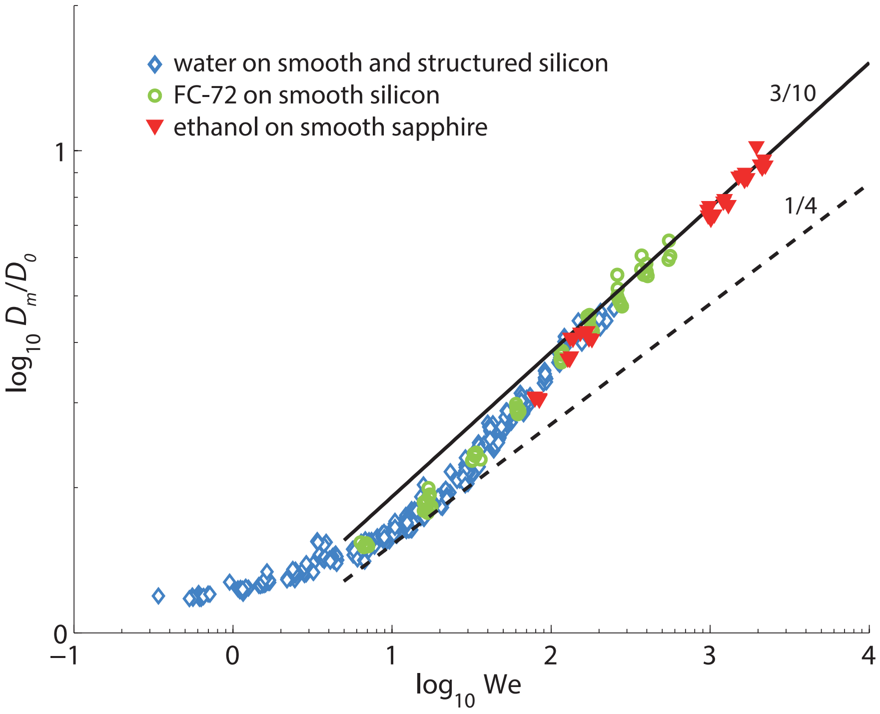

Figure 4.12: Maximum deformation of droplets impacting on superheated sapphire (red triangles) compared to the spreading factor of impacting drops taken from Tran *et al.* [16]. Blue triangles indicate water drops impacting on smooth and structured silicon and green circles are drops of FC-72 impinging smooth silicon. The deformation, D_m, is scaled with initial droplet diameter D_0. The 3/10 and 1/4 scaling laws are described in section 2.3 [14, 16].

Chapter 5

Conclusions

Impacting ethanol droplets on a smooth surface with varying surface temperature were studied. When the surface is heated above the liquid's boiling point, the droplet either comes into contact with the surface (the *contact* regime) or it is separated from the surface by a vapor film (the *film* regime). The critical temperature is called the dynamic Leidenfrost temperature and by means of a laser interferometry technique a clear distinction is made between both regimes. This temperature is taken to be the same for all Weber numbers in this research, despite the fact that it is known to be increasing for increasing We (Tran *et al.* [13]). Therefore it is recommended to extend the number of measurements between $T = 150$ and 175 °C to verify this dependence on We.

Increasing the droplet's impact velocity may lead to splash and for both the *contact* and *film* regime the transition to splash is determined experimentally, resulting in a detailed phase diagram consisting of four splashing regimes. Both transitions are found to be dependent on the temperature of the surface. The transition to splash in the *contact* regime, however, is different as compared to that of the *film* regime, as the critical We decreases. The transitions are described theoretically in a successful way by extending the model from Xu *et al.* [10] with the incorporation of the liquid-vapor phase transition.

Droplets which are bouncing or producing a stable liquid film at a high temperature, spread until a maximum spreading D_m is reached. It is shown that the maximum spreading factor Γ, which is the maximum spreading normalized by the droplet's initial diameter D_0, follows the scaling law presented by Tran *et al.* [16]. The experimental data for high Weber numbers was shown to be in line with this scaling law for the spreading factor $\Gamma \sim \mathrm{We}^{3/10}$, which is explained by taking into account the drag force of the vapor flow which is exerted on the liquid.

Bibliography

[1] R. Rioboo, C. Tropea, and M. Marengo. Outcomes from a drop impact on solid surfaces. *Atomization and sprays*, 11, 2001.

[2] A.M. Worthington. On the forms assumed by drops of liquids falling vertically on a horizontal plate. *Proceedings of the Royal Society of London Series A*, 25, 1876.

[3] S. Mandre, M. Mani, and M.P. Brenner. Precursors to splashing of liquid droplets on a solid surface. *Physical Review Letters*, 102, 2009.

[4] S. Mandre and M.P. Brenner. The mechanism of a splash on a dry solid surface. *Journal of Fluid Mechanics*, 690, 2012.

[5] C.D. Stow and M.G. Hadfield. An experimental investigation of fluid flow resulting from the impact of a water drop with an unyielding dry surface. *Proceedings of the Royal Society of London*, 373, 1981.

[6] Z. N. Wu. *Modélisation et calcul implicite multidomaine découlements diphasiques gaz-gouttelettes.* PhD thesis, Université Pierre et Marie Curie, Paris, France, 1992.

[7] C. Mundo, M. Sommerfeld, and C. Tropea. Droplet-wall collisions: experimental studies of the deformation and breakup process. *International Journal of Multiphase Flow*, 21, 1995.

[8] G.E. Cossali, A. Coghe, and M. Marengo. The impact of a single drop on a wetted solid surface. *Experiments in Fluids*, 22, 1996.

[9] K. Range and F. Feuillebois. Influence of surface roughness on liquid drop impact. *Journal of Colloid and Interface Science*, 203, 1998.

[10] L. Xu, W.W. Zhang, and S.R. Nagel. Drop splashing on a dry smooth surface. *Physical Review Letters*, 94, 2005.

[11] A.-L. Biance, C. Clanet, and D. Quéré. Leidenfrost drops. *Physics of Fluids*, 15, 2003.

[12] D. Quéré. Leidenfrost dynamics. *Annual Review of Fluid Mechanics*, 45, 2013.

[13] T. Tran, H.J.J. Staat, A. Prosperetti, C. Sun, and D. Lohse. Drop impact on superheated surfaces. *Physical Review Letters*, 108, 2012.

[14] C. Clanet, C. Béguin, D. Richard, and D. Quéré. Maximal deformation of an impacting drop. *Journal of Fluid Mechanics*, 517, 2004.

[15] P. Tsai, M.H.W. Hendrix, R.R.M. Dijkstra, L. Shui, and D. Lohse. Microscopic structure influencing macroscopic splash at high weber number. *Soft Matter*, 7, 2011.

[16] T. Tran, H.J.J. Staat, A. Susarrey-Arce, T.C. Foertsch, A.J. van Houselt, J.G.E. Gardeniers, A. Prosperetti, D. Lohse, and C. Sun. Droplet impact on superheated micro-structured surfaces. *Soft Matter*, 9, 2013.

[17] D. Richard and D. Quéré. Bouncing water drops. *Europhysics Letters*, 50, 2000.